Published in final edited form as:
*Nat Chem Biol*. 2016 February ; 12(2): 94–101. doi:10.1038/nchembio.1988.

# An *in vivo* platform for identifying inhibitors of protein aggregation

**Janet C. Saunders**[#1,2], **Lydia M. Young**[#1,2], **Rachel A. Mahood**[1,2], **Matthew P. Jackson**[1,2], **Charlotte H. Revill**[1,3], **Richard J. Foster**[1,3], **D. Alastair Smith**[4], **Alison E. Ashcroft**[1,2], **David J. Brockwell**[1,2,*], and **Sheena E. Radford**[1,2,*]

[1]Astbury Centre for Structural Molecular Biology, University of Leeds, Leeds, LS2 9JT, UK

[2]School of Molecular and Cellular Biology, University of Leeds, Leeds, LS2 9JT, UK

[3]School of Chemistry, University of Leeds, LS2 9JT, UK

[4]Avacta Analytical plc, Wetherby, LS23 7FZ, UK

[#] These authors contributed equally to this work.

## Abstract

Protein aggregation underlies an array of human diseases, yet only one small molecule therapeutic has been successfully developed to date. Here, we introduce an *in vivo* system, based on a β-lactamase tripartite fusion construct, capable of identifying aggregation-prone sequences in the periplasm of *Escherichia coli* and inhibitors that prevent their aberrant self-assembly. We demonstrate the power of the system using a range of proteins, from small unstructured peptides (islet amyloid polypeptide and amyloid β) to larger, folded immunoglobulin domains. Configured in a 48-well format, the split β-lactamase sensor readily differentiates between aggregation-prone and soluble sequences. Performing the assay in the presence of 109 compounds enabled a rank ordering of inhibition and revealed a new inhibitor of IAPP aggregation. This platform can be applied to both amyloidogenic and other aggregation-prone systems, independent of sequence or size, and can identify small molecules or other factors able to ameliorate or inhibit protein aggregation.



[*]Corresponding authors: D.J.Brockwell@leeds.ac.uk and S.E.Radford@leeds.ac.uk.

Author Contributions

J.C.S. and L.M.Y. contributed equally to this work. J.C.S. designed the study, purified the β-lactamase constructs, performed the *in vivo* experiments, performed the β-lactamase activity assays *in vitro*, performed TEM, analyzed results and wrote the manuscript. L.M.Y. conceived, designed and performed mass spectrometry experiments, performed TEM and thioflavin T fluorometry and analyzed results. R.A.M purified Aβ40 and performed TEM and thioflavin T fluorometry. M.P.J performed Western blots, dot blots, thioflavin T and NIAD-4 fluorometry. C.H.R. and R.J.F. designed and prepared the small molecule screening library. R.J.F also performed all PAINS analyses. D.A.S. contributed to experiment design. A.E.A. conceived and designed mass spectrometry experiments. D.J.B. and S.E.R. conceived and designed the experiments and wrote the manuscript. All authors contributed to manuscript preparation.

Competing financial interests

The authors declare no competing financial interests.


Europe PMC Funders Author Manuscripts

## Introduction

Preventing protein aggregation is of paramount importance in our quest to alleviate some of the most prevalent diseases in the developed world, from neurodegenerative disorders including Alzheimer's and Parkinson's diseases, to systemic disorders such as type II diabetes mellitus[1]. The key pathological hallmark of amyloid diseases is the accumulation of aggregated proteins in fibrillar structures known as amyloid[2]. The majority of studies of amyloid diseases suggest that the most toxic species are low molecular weight soluble oligomers, or higher molecular weight prefibrillar intermediates that form en route to fibrils[2], although fibrils themselves may also play a contributing role[3, 4].

One approach to prevent protein aggregation is to bind small molecules specifically to the precursor protein of interest and hence inhibit the initial stages of misfolding and self-assembly[5]. As many aggregation-prone proteins are intrinsically disordered, structure-based design strategies are not always possible. Identification of small molecules that prevent protein aggregation by *in vitro* screening methods commonly requires the demanding purification of the aggregation-prone precursor protein in high yield for subsequent biophysical analysis, e.g. using the fluorescence of thioflavin T (ThT) or analysis by electron microscopy (EM) or other spectroscopic methods. Such analyses, however, are slow, laborious and can lead to false positive results[6]. Furthermore, synthetic peptide samples can be difficult to produce in a form that is free of oligomeric 'seeds' that can nucleate further aggregation[7]. The presence of these pre-existing oligomers during inhibitor screening could lead to some of the most important inhibitors, those that prevent low molecular weight oligomer formation, being overlooked.

Here we describe a powerful sensor for detecting the aggregation of proteins into both amyloid and amorphous aggregates and its inhibition by small molecules. Taking the form of a β-lactamase tripartite fusion construct[8], the sensor directly links the aggregation-propensity of a test protein in the periplasm of *E. coli* to a simple phenotypic readout: antibiotic resistance. We show that the system can be used to detect aggregation-prone sequences and to screen for inhibitors that prevent protein aggregation, using human and rat islet amyloid polypeptide (hIAPP and rIAPP, respectively), amyloid β 1–40 (Aβ40), amyloid β 1–42 (Aβ42), $\beta_2$microglobulin ($\beta_2$m) and its amyloid variant D76N and the domain antibodies HEL4 and Dp47d as examples. The *in vivo* system described enables facile analysis of protein aggregation and its inhibition, without requiring any prior knowledge of the protein's structure or function.

## Results

### Rationale for the periplasmic-based screen

Previous studies have shown the potential of using bacterial- or yeast-based systems to screen for small molecule inhibitors of protein aggregation[9-14]. The systems reported to date, however, have been limited to the reducing environment of the cytosol, preventing analysis of disulfide bond-containing proteins, which comprise > 50 % of proteins involved in pathologic amyloid disease[1]. Another critical limitation of cytoplasmic-based screens is the restrictive nature of biological membranes, limiting their application to the identification

of molecules that can traverse this barrier. The work described here obviates these drawbacks by performing a screen for inhibitors of protein aggregation within the oxidizing periplasmic space of *E. coli*. Therein, disulfide bond formation is permitted and the presence of outer membrane porins allows diffusive access to molecules up to ~ 600 Da[15]. In the aggregation sensor described, the test sequence is inserted between two domains of the periplasmic-based reporter enzyme TEM-1 β-lactamase (Figs. 1a, b). Upon correct folding of the test protein in the periplasm of *E. coli*, the two halves of β-lactamase are brought into close proximity and form a functional enzyme, enabling the bacteria to be resistant to β-lactam antibiotics (Fig. 1c). This β-lactamase tripartite fusion system has been used previously to identify protein variants with increased thermodynamic stability, to identify new periplasmic chaperones and to develop excipients that stabilize proteins thermodynamically[8, 16, 17]. The assumption of the assay described here is that if the test protein aggregates, the β-lactamase domains will be prevented from associating, and/or the active enzyme will be removed from the periplasm by degradation, leading to *E. coli* with increased sensitivity to β-lactam-containing antibiotics (Fig. 1d). When the bacteria are grown in the presence of small molecule inhibitors of protein aggregation, antibiotic resistance should be restored in a quantitative manner (Fig. 1e).

## Identification of aggregation-prone sequences

To demonstrate that the antibiotic resistance conferred by the tripartite β-lactamase fusion sensor can be used to monitor protein aggregation *in vivo*, four test proteins with different aggregation propensities were selected: hIAPP, rIAPP, Aβ40 and Aβ42 (Supplementary Results, Supplementary Fig. 1a). Aβ40 and Aβ42, peptides involved in Alzheimer's disease, are highly aggregation-prone and were chosen for analysis based on their rapid, *in vitro* aggregation rates[18, 19]. hIAPP, the aggregating protein in type II diabetes mellitus, shares 24 % sequence identity and 46 % similarity with Aβ42 (Supplementary Fig. 1b) and is also highly aggregation-prone[20]. hIAPP also contains a disulfide bond that plays a role in the fibril assembly mechanism[21]. By contrast, rIAPP shares 84 % sequence identity with hIAPP, but is not amyloidogenic[20]. This sequence thus provides a useful control for the aggregation screen.

The antibiotic resistance conferred by the four β-lactamase test protein constructs was determined in a 48-well agar plate assay. The test proteins were cloned into a 28-residue glycine/serine-rich linker (βla-linker$_{SHORT}$) between residues 196 and 197 of TEM-1 β-lactamase (Figs. 1a, b, Supplementary Tables 1 and 2) and the antibiotic resistance of *E. coli* expressing each of the constructs was measured as the maximal cell dilution at which colony growth was observed to occur (MCD$_{GROWTH}$, see online Methods) after 18 h over a range of ampicillin concentrations (0–140 μg/mL). A non-aggregating control (β-lactamase containing a 64-residue glycine/serine linker, similar in length to the 65–70 residue combined length of the Aβ/IAPP-G/S linker in the sensor constructs) was also analyzed (βla-linker). The spot titers comparing the growth of the strains expressing the different constructs at a single concentration of ampicillin (80 μg/mL) are depicted in Fig. 1f. The results showed that bacteria expressing the non-aggregating glycine/serine-rich linker (βla-linker) and rIAPP (βla-rIAPP) constructs grew at significantly higher cell dilutions (Fig. 1f) and at higher concentrations of ampicillin (Fig. 1g) than the strains expressing the

aggregating constructs (βla-hIAPP, βla-Aβ40 and βla-Aβ42). As the glycine/serine linker, rIAPP, hIAPP, Aβ40 and Aβ42 are all intrinsically disordered[22, 23], the reduced enzymatic activity of β-lactamase presumably results from aggregation *in vivo* and cannot be attributed to the presence of an extended loop region separating the two domains of β-lactamase. Furthermore, the reduced β-lactamase activity observed for βla-Aβ40/42 and βla-hIAPP cannot be explained by differential expression as Western blot analysis showed that all constructs expressed to a similar level (Supplementary Fig. 2a). However, for all proteins except βla-linker, the majority of the protein was insoluble (Supplementary Fig. 2b). The data show, therefore, that the split β-lactamase system can be used as a sensor for protein aggregation *in vivo*.

## Protein aggregation correlates with antibiotic resistance

The extent of antibiotic resistance observed for the different β-lactamase constructs *in vivo* was next compared with the amyloid growth profile of the test peptides *in vitro* in the absence of the β-lactamase scaffold. Thioflavin T (ThT) fluorescence over 24 h (Fig. 2a) and transmission electron microscopy (TEM) images (taken after 5 days of incubation, Fig. 2b) showed that amyloid fibrils were formed by hIAPP, Aβ40 and Aβ42, but not rIAPP, as expected[18-20]. These data show a correlation between the rate of amyloid formation observed by ThT fluorescence for the isolated peptides and the level of antibiotic resistance revealed by the *in vivo* sensor assay (compare Fig. 2a and Fig. 1g). Importantly, rIAPP, which does not form amyloid fibrils (Fig. 2a) but instead forms small spherical aggregates *in vitro* (Fig. 2b), did not result in significantly reduced antibiotic resistance (at ampicillin concentrations < 60 μg/mL) compared with the βla-linker construct (Fig. 1g). Conversely, the three amyloidogenic peptides, hIAPP, Aβ40 and Aβ42, formed long straight fibrillar structures (Fig. 2b), and significantly reduced the ampicillin resistance of bacteria containing these sequences in the tripartite β-lactamase sensor (Fig. 1g).

The progress of aggregation of each of the four peptides was also investigated using electrospray ionisation-mass spectrometry linked to ion mobility spectrometry (ESI-IMS-MS)[24]. The resulting Driftscope plots represent a snap-shot of the species present in solution at a given time point during the aggregation process. At t = 2 min, monomeric through to hexameric species were observed for both rIAPP and hIAPP, consistent with previous results (Fig. 2c)[20]. The intensity of these oligomers remained similar after 24 h (Fig. 2d), suggesting that although aggregation is occurring (into low-order aggregates or fibrils, for rIAPP and hIAPP, respectively), the reaction had not yet reached completion. In the case of Aβ40, at t = 2 min monomeric through to pentameric species were observed (Fig. 2c). After 24 h, the rapid aggregation of this peptide resulted in the consumption of higher order species such that only monomer through to trimer remained (Fig. 2d). For Aβ42, the most aggregation-prone of the four peptide sequences studied[18], aggregation occurred at such a rate that oligomers were difficult to observe by ESI-IMS-MS. As early as t = 2 min (Fig. 2c), no higher order (> tetrameric) oligomers were observed under the conditions of this experiment, with only monomers and dimers remaining after 24 h (Fig. 2d).

The data reveal a correlation between the *in vivo* antibiotic sensitivity of each β-lactamase construct and the aggregation propensity of the test peptides *in vitro*. To determine the effect

of the incorporation of the peptide sequences into the β-lactamase scaffold on their aggregation propensity *in vitro*, βla-hIAPP and βla-linker were expressed recombinantly and the ability of the resulting purified proteins to aggregate was measured. After 5 days incubation, 66 % of βla-hIAPP could be pelleted by centrifugation (Fig. 3a) and the specific enzyme activity of the whole sample had decreased by 74 % (Fig. 3b, specific activity at 0 days = 226 ± 9 μmol/min/mg enzyme, defined as 100 %). The data demonstrate, therefore, that insertion of the hIAPP sequence causes the aggregation of the β-lactamase construct, rendering it inactive. The aggregates formed by βla-hIAPP *in vitro* are amyloid-like, demonstrated by binding of the amyloid-specific dyes NIAD-4[25] and ThT (Supplementary Fig. 3a, b), their appearance as long, straight fibrils, observed by negative-stain TEM (Supplementary Fig. 3c), and recognition by the amyloid fibril-specific antibody WO1[26] (Supplementary Fig. 3d). Notably, no aggregation or amyloid formation was detected under the same conditions for the βla-linker construct (Figs. 3a, b and Supplementary Fig. 3). This demonstrates that although the termini of hIAPP are joined to the β-lactamase linker, the hIAPP sequence is still able to cause amyloid formation of the intact βla-hIAPP construct.

We next examined the ability of the tripartite fusion system to distinguish between aggregation-prone and aggregation-resistant proteins using the larger, globular disulfide bond-containing immunoglobulin (Ig) domain of wild-type (WT) human $\beta_2$m and its naturally occurring variant D76N (11.9 kDa, 100 residues) (Supplementary Fig. 4a). WT $\beta_2$m does not form amyloid fibrils *in vitro* at neutral pH[27], whereas D76N $\beta_2$m readily aggregates and causes systemic amyloid disease[28, 29]. In addition, the effect of the insertion of biopharmaceutically-relevant domain antibodies (dAbs) on antibiotic resistance was also examined, by the creation of constructs containing the soluble dAb HEL4 (12.9 kDa, 120 residues) and its aggregation-prone counterpart, Dp47d (a human $V_H$ dAb encoded by the same germline gene as HEL4 but differing in 41 residues; 12.4 kDa, 116 residues)[30] (Supplementary Fig. 4b). Unlike the other test proteins selected, Dp47d rapidly aggregates *in vitro* into amorphous aggregates[31]. The antibiotic resistance of bacteria expressing either of the aggregation-prone variants (βla-$\beta_2$m-D76N or βla-Dp47d) was significantly lower at all ampicillin concentrations studied than their non-aggregating counterparts (Supplementary Fig. 4c, d). The data demonstrate the capability of the tripartite fusion system to detect aggregation- and non-aggregation-prone variants ranging in size (3.9–12.9 kDa), structure (natively disordered or folded), and aggregation properties (amyloid *versus* non-specific aggregation). Previous studies using the tripartite system described to evolve protein stability *in vivo* have demonstrated the ability to insert larger proteins (maltose binding protein, 42.5 kDa) into the linker region of β-lactamase[8], indicating that the system could be used for even larger aggregation-prone variants than those demonstrated in this study.

## Protein aggregation inhibitors rescue bacterial growth

To demonstrate that the β-lactamase tripartite sensor can be used as a screen for small molecule discovery, the *in vitro* aggregation experiments using βla-hIAPP were repeated in the presence of a 10-fold molar excess of the known inhibitor of hIAPP aggregation, curcumin[32, 33] (compound **1**, Supplementary Data Set 1, Supplementary Table 3). This compound prevented βla-hIAPP aggregation *in vitro*, as indicated by retention of βla-hIAPP in solution in a catalytically active form (Figs. 3b, c). Importantly, the control βla-linker did

not aggregate in the absence or presence of curcumin (Fig. 3a, c), and the presence of curcumin did not affect the specific activity of this non-aggregating control (Fig. 3b). The ability of βla-hIAPP to bind curcumin was corroborated further by ESI-MS (Supplementary Fig. 5), and TEM analysis of the samples at the end of the 5 day incubation showed a lack of fibrillar material in the presence of curcumin, but not in its absence (Fig. 3d). The ability of curcumin to prevent βla-hIAPP aggregation *in vivo* was then demonstrated by increased maximal cell dilution allowing growth ($MCD_{GROWTH}$) values over a range of ampicillin concentrations (0–140 μg/mL) (Fig. 3e), once the effect of curcumin on bacterial growth was accounted for (using the non-aggregating control βla-linker, see online Methods and Supplementary Fig. 6). To obtain a single value that showed the effect of the small molecule on bacterial growth, the ratio of the $MCD_{GROWTH}$ values of the treated versus untreated samples was calculated from the area under the antibiotic survival curves and plotted as $\log_2$(treated/untreated) (Fig. 3f). This approach identifies any small molecule with a $\log_2$ score > zero as a 'hit' in the *in vivo* screen, with full (100 %) rescue of bacterial growth for βla-hIAPP compared with βla-linker giving a $\log_2$(treated/untreated) score of 1.2. The results show, therefore, that growth of βla-hIAPP-expressing bacteria is restored in the presence of curcumin in a dose-dependent manner, with full rescue from βla-hIAPP aggregation occurring at ≥ 200 μM curcumin (Fig. 3f).

## System detects inhibitors of hIAPP aggregation *in vivo*

Having established a system capable of detecting inhibition of βla-hIAPP aggregation *in vivo*, we next built on our previous results (using a synthetic peptide of hIAPP)[24] by repeating the *in vivo* sensor assay in the presence of nineteen additional small molecules with known effects on the aggregation of hIAPP (Supplementary Table 3, compounds **2–20**; Supplementary Data Set 1). Five of these molecules (acid fuchsin[34, 35], EGCG[20, 24, 36], Fast green FCF[24, 35], caffeic acid[37] and silibinin[20, 38]), together with curcumin[32, 33], have been shown to inhibit hIAPP amyloid formation *in vitro*, ten compounds (hemin[24], resveratrol[39], 1*H*-B-SA[24], benzimidazole[24], tramiprosate[24], aspirin[24], Congo red[24], azure A, thiabendazole and Orange G (Supplementary Table 3)) do not prevent hIAPP aggregation, and four compounds (acridine orange[40], myricetin[41, 42], phenol red[43, 44] and morin hydrate[45]) have been suggested as inhibitors of hIAPP aggregation *in vitro*, but with either incomplete or equivocal results. A concentration of 100 μM small molecule was chosen to minimize any inherent cellular toxicity of the compounds and the $\log_2$(treated/untreated) scores were calculated (Fig. 4a). Five of the published inhibitors of hIAPP aggregation (curcumin, acid fuchsin, EGCG, Fast green FCF and caffeic acid), and one compound with conflicting results (acridine orange), were clear hits in the *in vivo* screen (Fig. 4a). The single false negative observed in the screen was the small molecule silibinin which inhibits hIAPP aggregation *in vitro*[20], but had no protective effect in the *in vivo* assay (Fig. 4a). However, when the concentration of silibinin was increased, βla-hIAPP aggregation was prevented *in vivo* (Supplementary Fig. 7a). By contrast, increasing the concentration of a compound that had no effect on bacterial growth at 100 μM (benzimidazole) up to 1,000 μM did not rescue bacterial sensitivity to ampicillin (Supplementary Fig. 7b). Two compounds (myricetin and phenol red) were partial hits, while the remaining eleven molecules had no restorative effect on cell growth (Fig. 4a). It is noteworthy that $\log_2$(treated/untreated) scores

in the presence of the latter set of compounds are negative. This suggests that the effects of aggregation and ampicillin on cell viability are not independent.

The *in vitro* aggregation propensity of hIAPP peptide in the absence (Fig. 4b) or presence (Fig. 4c–f, Supplementary Table 4) of each of the twenty small molecules tested was also investigated using ESI-IMS-MS[20, 24] and TEM. In the absence of small molecule inhibitors of aggregation, hIAPP formed up to hexameric oligomers (within 2 min of dilution into buffer), as observed by ESI-IMS-MS[20, 24] (Fig. 4b Driftscope), and fibrils were observed after 5 days incubation (Fig. 4b TEM). Five 'hits' from the *in vivo* screen (curcumin, acid fuchsin, EGCG, Fast green FCF and acridine orange) bound to hIAPP specifically at a 10-fold molar excess (Fig. 4c and Supplementary Table 4 ESI mass spectra), prevented or retarded oligomer formation (Fig. 4c Driftscope, Supplementary Table 4) and inhibited fibril formation (Fig. 4c TEM, Supplementary Table 4). The partial hits from the *in vivo* screen, myricetin and phenol red, bound non-specifically (multiple ligands bound) to hIAPP and did not prevent formation of aggregated material (Fig. 4d and Supplementary Table 4). Conversely, the twelve small molecules that failed to prevent βla-hIAPP aggregation in the *in vivo* screen (Fig. 4a) either did not bind (Fig. 4e), or bound non-specifically or colloidally (self-association of small molecule, Fig. 4f) to hIAPP *in vitro*, resulting in the formation of amyloid fibrils or large amorphous aggregates (Figs. 4e, 4f, Supplementary Table 4). Similar results were obtained using βla-hIAPP in the presence of the same small molecules (Fig. 4b–f TEM).

## Screen identifies a new inhibitor of hIAPP aggregation

The screen detailed above was performed in 48-well agar plate format and requires ~ 0.5 mg small molecule per assay. To increase throughput and to minimize the amount of small molecule required the screen was repeated, using the same twenty test molecules, at a single concentration of ampicillin (100 μg/mL) and small molecule (100 μM), thereby requiring only ~ 0.07 mg of compound (online Methods and Supplementary Fig. 8). Any intrinsic effect of each small molecule on bacterial growth was accounted for by determining the effect of the same concentration of small molecule on the growth of βla-linker at 100 μg/mL ampicillin. Consistent with the results in Fig. 4a, the same six small molecules able to prevent βla-hIAPP aggregation were identified using the miniaturized assay (Supplementary Fig. 9, compounds **1–6**). To further demonstrate the feasibility of a larger scale screen, an additional thirty compounds that we have previously shown to inhibit or have no effect on hIAPP aggregation *in vitro* using ESI-MS and TEM[24] were screened in the miniaturized *in vivo* assay using an ampicillin concentration of 100 μg/mL (Supplementary Data Set 1, Supplementary Fig. 9, compounds **21–50**). The results were entirely consistent between the *in vitro* and *in vivo* assays with only one small molecule previously shown to bind specifically to hIAPP (using ESI-MS) and prevent fibril formation *in vitro*[24] resulting in a positive score in the *in vivo* assay (compound **36**, named here JCS-1).

In the quest to identity a new inhibitor of hIAPP aggregation, an additional fifty-nine compounds were chosen to assay against hIAPP aggregation *in vivo*. Thirty-one of the chosen compounds are known to interact with, and/or prevent, aggregation of other proteins (Supplementary Data Set 1 compounds **51–81**) and a further twenty-eight compounds were

selected through focused screening using Rapid Overlay of Chemical Structures (ROCS), a method that improves the hit-rate of high throughput screening (HTS) (Supplementary Data Set 1 compounds **82–109**). These compounds were selected for analysis based on their structural similarities to the inhibitor of hIAPP aggregation identified previously, JCS-1 (compound **36**)[24]. From these fifty-nine compounds, one compound significantly aided growth (compound **56** (dopamine); Supplementary Figs. 10 and 11; $\log_2$(treated/untreated) = 0.75), while five compounds were identified which moderately aided bacterial growth ($\log_2$(treated/untreated) = 0.24; compounds **52** (apomorphine), **84** (JCS-2), **94** (JCS-3), **100** (JCS-4) and **103** (JCS-5); Supplementary Fig. 10). The ability of the five moderate hit compounds to prevent hIAPP aggregation was confirmed by analysis of increasing concentrations of each small molecule on bacterial growth (Supplementary Fig. 12), combined with TEM (Supplementary Fig. 12) and ESI-IMS-MS analysis (Supplementary Fig. 13). When the *in vivo* assay was repeated over the original full range of ampicillin concentrations (0–140 μg/mL) in the presence of increasing concentrations of the strong hit dopamine, bacterial growth was rescued in an approximately dose-dependent manner (Fig. 5a, b). Dopamine is known to reduce fibril formation of Aβ[46] and α-synuclein (the protein associated with Parkinson's disease)[46, 47] by driving the aggregation pathway towards the formation of non-fibrillar oligomers or small protofilaments. hIAPP treatment with a 10-fold excess of dopamine led to the formation of small amorphous aggregates (Fig. 5c) and ESI-IMS-MS analysis confirmed that dopamine binds specifically to hIAPP (Fig. 5d), preventing high order oligomer formation (Fig. 5e).

Finally, the hydrophobicity (LogP, the logarithm of the hydrophobic partition coefficient) and molecular weight of the newly identified small molecule inhibitors were compared with all other small molecules in our screen. Importantly, the results (Supplementary Figs. 14 and 15) showed that the *in vivo* assay does not simply identify small or hydrophobic compounds. In addition, analysis of the properties of these compounds as pan-assay interference compounds (PAINS), small molecules that can lead to aberrant identification of leads based on promiscuous binding, covalent modification of the target, small molecule reactivity, chemical aggregation or fluorescence[48, 49], identified two of the five newly identified inhibitors as potential PAINS molecules (apomorphine and dopamine, compounds **52** and **56**, respectively; Supplementary Data Set 1). Importantly, by analyzing all of the compounds from our *in vivo* screen using ESI-IMS-MS (Supplementary Table 4 and Supplementary Fig. 13) we are able to rule out any degradation of the compound, covalent attachment or chemical modification of hIAPP based upon the mass of each species present.

## Discussion

Current *in vitro* techniques for investigating protein aggregation and its inhibition can be costly, time consuming and require large quantities of often difficult to purify proteins. Here, we describe a facile approach for screening protein aggregation propensity and its inhibition in the periplasm of *E. coli*. The system has multiple benefits: i) it is able to detect and quantify the extent of protein aggregation *in vivo* via a simple readout of antibiotic resistance; ii) it can be used to screen for inhibitors of aggregation; and iii) it is applicable to proteins of different sizes and structure, with or without disulfide bonds and different aggregation propensities (amyloid or non-specific aggregation into large assemblies). We

show that the system reports reliably on the aggregation of four test proteins that are intrinsically disordered (rIAPP, hIAPP, Aβ40 and Aβ42) and four that are stably folded Ig domains (WT $\beta_2$m, D76N $\beta_2$m, HEL4 and Dp47d).

A powerful use of the periplasmic-based assay described is its ability to screen for small molecule inhibitors of aggregation. Here, we demonstrate this principle by describing a selection of 109 small molecules against the aggregation of hIAPP, both *in vivo* and *in vitro*. To enable large pools of potential aggregation inhibitors to be screened against a protein target, we have also miniaturized the assay to make it amenable to high throughput format, using just ~ 0.07 mg of test compound. Indeed, this enabled the discovery of dopamine as an inhibitor of hIAPP aggregation.

The ability to distinguish aggregation-prone variants from their non-aggregating counterparts *in vivo* suggests that the system developed could be used to study the aggregation propensity of mutants of aggregation-prone proteins without the requirement to first purify each variant. As the readout of the *in vivo* assay is independent of the activity, size or structure of the inserted test protein, it obviates the need to develop individual assays for different test proteins to determine their aggregation levels. The tripartite sensor also avoids the use of ThT, which can lead to erroneous results[6]. The tripartite system described here has previously been used to evolve protein stability *in vivo*, which demonstrated the ability to insert large proteins (maltose binding protein, 43 kDa) into the linker region of β-lactamase[8]. In combination with the data presented here, this validates the utility of the assay for analysis of large protein systems, as well as proteins that are intrinsically disordered or initially folded, as well as for proteins that form ordered aggregates such as amyloid, or form amorphous aggregates, including candidate biopharmaceuticals. Whether the system can also detect aggregation into oligomers for different systems, including those proposed to be cytotoxic, remains to be determined. However, the observation that bacteria expressing βla-rIAPP grow less well than βla-linker (at > 60 μg/mL ampicillin, Fig. 1g), suggests that small oligomeric states may indeed impart a deleterious effect on β-lactamase activity in the absence of large aggregates. This difference in growth is more pronounced at higher concentrations of ampicillin than used in this study, demonstrating that tuning of the ampicillin concentration range for the aggregating system of interest may enable identification of smaller aggregated species than those shown here. As with other screening techniques for small molecule inhibitors of protein aggregation, it is essential to analyse potential hits from the *in vivo* screen using additional biophysical analyses. Here we show the powers of ESI-IMS-MS for such analysis in its capability not only to distinguish specific from non-specific or colloidal binding[24], but also to determine the effect of ligand binding on the oligomeric species formed. The *in vivo* sensor, in conjunction with ESI-IMS-MS and TEM, could also be used, therefore, to identify compounds that arrest aggregation at different assembly stages, providing novel compounds with defined properties for the determination of toxic or benign intermediate species.

The inherent ability of proteins to aggregate into amyloid fibrils underlies more than fifty human diseases[1]. With our ageing population, the social and economic burdens on patients and society are expected to increase dramatically over the coming years. To date, only one successful small molecule therapeutic targeting an amyloid disease has been developed[5]. As

the complex nature of these diseases may demand a multi-pronged attack, identification of protein aggregation inhibitors is a vital step towards therapeutic alleviation of these devastating diseases. Moreover, at a fundamental level, the discovery of small molecules able to trap aggregating proteins at defined points, made possible by combining the tripartite system and ESI-IMS-MS analysis, will provide new opportunities to understand how and why proteins form amorphous aggregates or self-assemble into amyloid. We envisage, therefore, that the β-lactamase tripartite fusion system will play a valuable role in our quest to develop small molecules able to arrest amyloid formation, as well as to prevent aggregation of other valuable proteins, including protein-based pharmaceuticals.

## Online Methods

### Small molecules

All small molecules were > 98 % pure and were purchased from Sigma-Aldrich Co. Ltd, except for 4,5-dihydroxy-2,7-naphthalenedisulfonic acid, acid fuchsin, acridine orange, calmagite, Fast green FCF, methyl yellow, phenol red and rhodamine B (Fisher Scientific); and Basic blue 41, resveratrol and tramiprosate (Santa Cruz Biotech). The 28 compounds selected using ROCS *Combiscore* were obtained from an in-house library of small molecules at the University of Leeds, UK and were > 95 % pure (by LCMS and $^{1}$H NMR analysis).

### Cloning test proteins into β-lactamase linker

Plasmids containing the genes encoding β-lactamase with a 28-residue glycine/serine (G/S)-rich linker (pMB1-βla-linker$_{SHORT}$) and β-lactamase with a 64-residue G/S linker (pMB1-βla-linker$_{LONG}$) were kindly provided by Prof. Jim Bardwell (Department of Biological Chemistry, University of Michigan, USA)[8].

Genes encoding the test proteins were cloned into the 28-residue G/S linker that had previously been inserted between residues 196 and 197 of TEM-1 β-lactamase[8] (Supplementary Table 1). PCR was performed to amplify the hIAPP, rIAPP, Aβ42 and WT-$\beta_2$m genes from the plasmids pTXB1-hIAPP[51], pTXB1-rIAPP[51] (both kindly provided by Prof. Andrew Miranker, Yale University), pRSET-Aβ40/42[52] (kindly provided by Prof. Sarah Linse, Lund University) and pET23a-WT-$\beta_2$m[53]. The primers were designed to encode XhoI and BamHI restriction sites 5′ and 3′ to the genes, respectively (see Supplementary Table 2 for primers) as these are the restriction sites in βla-linker$_{SHORT}$. Synthetic genes encoding HEL4 or Dp47d with an XhoI restriction site 5′ and BamHI restriction site 3′ to the genes were purchased from Eurofins Genomics. The plasmids containing βla-linker$_{SHORT}$, HEL4 and Dp47d, and the PCR products were digested with XhoI and BamHI. The sequences encoding the test proteins were ligated into the β-lactamase linker region and the ligation products were transformed into *E. coli* SCS1 cells (Stratagene) and the cells grown on agar plates containing 10 μg/mL tetracycline. Successful ligation was identified by the resistance to tetracycline obtained from the vector. Plasmid DNA was purified from a selection of colonies and was sequenced to confirm that plasmids contained the correct sequences. Primers for the sequencing reactions were designed to bind upstream and downstream of the GS linker of β-lactamase (Supplementary Table 2). The

newly synthesized plasmids were named βla-hIAPP, βla-rIAPP, βla-Aβ42, βla-WT-$\beta_2$m, βla-HEL4 and βla-Dp47d. The plasmid βla-Aβ40 was created using QuikChange mutagenesis (Agilent Technologies) by deleting the last two residues of the Aβ42 sequence that had been inserted into the β-lactamase linker (Supplementary Table 2). The plasmid βla-$\beta_2$m-D76N was created, using QuikChange mutagenesis, from the WT-$\beta_2$m sequence that had been inserted into the β-lactamase linker (Supplementary Table 2).

## $MCD_{GROWTH}$ assays

**Spot titer tests—**Spot titer tests were performed to determine the level of β-lactam antibiotic resistance of cells expressing the β-lactamase tripartite fusions. A single colony from fresh *E. coli* BL21 (DE3) cells (Stratagene) (transformed with the appropriate plasmid) was used to inoculate 100 mL sterile LB containing 10 μg/mL tetracycline (Formedium). Cultures were incubated overnight at 37 °C with shaking (200 rpm). 1 mL of overnight culture was used to inoculate 100 mL sterile LB containing 10 μg/mL tetracycline and grown at 37 °C (shaking at 200 rpm) until an $OD_{600}$ of 0.6 was reached. Expression of the β-lactamase fusion construct was induced by the addition of filter-sterilized arabinose (Sigma) to a final concentration of 0.02 % (*w*/*v*). Cultures were incubated for a further 1 h, when the $OD_{600}$ of the cells was adjusted to 1.0 using sterile LB, and the cultures were then serially diluted in 10-fold increments into sterile 170 mM NaCl solution. 3 μL of each dilution was then spotted onto LB agar plates, supplemented with 10 μg/mL tetracycline, 0.02 % (*w*/*v*) arabinose, and increasing concentrations of ampicillin (Formedium) (0–140 μg/mL). The plates were incubated at 37 °C for 18 h and the maximal cell dilution allowing cell growth ($MCD_{GROWTH}$) was determined for each ampicillin concentration by visual inspection.

## $MCD_{GROWTH}$ assay - full ampicillin range

Assays were performed in 48-well agar plates (Greiner Bio-One). 48-well plates containing the small molecule of interest were prepared prior to the assay using the following procedure. Two plates were prepared for each small molecule of interest, one for bacteria expressing the βla-$linker_{LONG}$ construct and one for bacteria expressing the βla-hIAPP construct. 3 μL of 10 mM small molecule (dissolved in DMSO, $H_2O$, or EtOH) was added to each well of two 48-well plates. Tetracycline (10 μg/mL final concentration) and filter sterilized arabinose (0.02 % *w*/*v* final concentration) were added to 100 mL of sterile 1.5 % (*w*/*v*) agar cooled to < 50 °C. 297 μL of this solution was then added into each of the first 6 wells (first row) of both 48-well plates. Plates were shaken (manually) to ensure mixing of the agar and small molecule. Ampicillin (10 mg/mL stock) was then added to the agar stock to give the required concentration for the next row of wells. This procedure was repeated until the plate contained 8 rows of agar containing increasing concentrations of ampicillin from 0–140 μg/mL (20 μg/mL increments). Agar plates were left to set in a sterile environment. The same procedure was followed to produce an additional two plates containing no small molecule (3 μL of solvent was added to the wells in place of small molecule).

*E. coli* BL21 (DE3) cells transformed with the appropriate plasmid were grown as described above until an $OD_{600}$ of 0.6 was reached. β-lactamase expression was then induced by the

addition of filter-sterilized arabinose to a final concentration of 0.02 % (*w*/*v*). 396 μL was removed and added to a 1.5 mL Eppendorf tube containing 4 μL of 10 mM small molecule (to give a final small molecule concentration of 100 μM). These cultures were incubated for a further 1 h, when the $OD_{600}$ of the cells was adjusted to 1.0 with LB medium and the culture then serially diluted 10-fold into sterile 170 mM NaCl solution. 3 μL of each dilution was then spotted onto the agar plates supplemented with the small molecule. The plates were incubated at 37 °C for 18 h and the $MCD_{GROWTH}$ was determined for each ampicillin concentration.

The intrinsic effect of each small molecule on bacterial growth was determined by comparing the growth *of E. coli* BL21 (DE3) cells transformed with βla-linker in the absence or presence of each small molecule. The effect of each small molecule on bacterial growth was subtracted from the β-lactamase-test protein assay, at each concentration of ampicillin. Example data are given in Supplementary Fig. 6.

In order to obtain a single value from each MIC assay, illustrative of the small molecule's effect on bacterial growth, the area under the MIC assay curves was calculated as a sum of the areas of 7 trapezia using equation (1), where $A_{curve}$ is the total area under the curve, and $x_i$ and $y_i$ are the *x*-axis and *y*-axis values at each concentration of ampicillin

$$A_{curve} = \sum_{i=1}^{7} \frac{y_i + y_{i+1}}{2} \times (x_{i+1} - x_i) \quad \text{(Equation 1)}$$

### $MCD_{GROWTH}$ assay – HTS format

Assays were performed in 48-well agar plates using a single concentration of small molecule (100 μM) and ampicillin (100 μg/mL)**.** Supplementary Fig. 8 shows a summary schematic of the technique. 48-well agar plates containing the small molecule of interest were prepared prior to the assay using the same technique described above, however ampicillin (100 μg/mL final concentration) was added to the agar prior to pouring the plates. Cultures were prepared as described previously.

### *In vivo* Western blot

A single colony from fresh *E. coli* BL21 (DE3) cells (transformed with the appropriate plasmid) was used to inoculate 100 mL sterile LB containing 10 μg/mL tetracycline. Cultures were incubated overnight at 37 °C with shaking (200 rpm). 1 mL of overnight culture was used to inoculate 100 mL sterile LB containing 10 μg/mL tetracycline and grown at 37 °C (shaking at 200 rpm) until an $OD_{600}$ of 0.6 was reached. 10 mL of culture was removed for the uninduced sample and centrifuged at 4,000 *g* for 10 min (4 °C). Expression of the β-lactamase fusion construct was induced by the addition of filter-sterilized arabinose to a final concentration of 0.02 % (*w*/*v*). Cultures were incubated for 1 h (37 °C, 200 rpm) and 10 mL was removed from each (induced sample). The 10 mL cultures were harvested by centrifugation at 4,000 *g* for 10 min (4 °C). The cell pellets (uninduced and induced with arabinose) were resuspended in phosphate buffered saline (PBS, Dulbecco's PBS, Sigma) to obtain an $OD_{600}$ of 5. For whole cell samples, 200 μL of the

$OD_{600}$ = 5 sample was combined with 200 μL PBS. 100 μL of 6 × loading dye (150 mM Tris-HCl, pH 6.8, 300 mM DTT, 6 % (*v*/*v*) SDS, 0.3 % (*w*/*v*) bromophenol blue) was then added. For soluble samples, 200 μL of the $OD_{600}$ = 5 sample was combined with 200 μL bacterial protein extraction reagent (ThermoFisher Scientific) and incubated with agitation for 10 min. The sample was then centrifuged at 16,000 *g* for 30 min (4 °C) and 100 μL of 6 × loading dye was added to the supernatant. The mixtures were then incubated at 90 °C for 10 min.

Protein samples were separated on an SDS PAGE gel (15 % (*v*/*v*) acrylamide, 0.4 % (*w*/*v*) *bis*-acrylamide, 1 M Tris-HCl, pH 8.45, 0.1 % (*w*/*v*) SDS) and were transferred to Amersham polyvinylidene fluoride membrane using a semi dry transfer apparatus (Bio-Rad Ltd). Blocking was performed for 3 h at room temperature using 5 % (*w*/*v*) milk powder in TBST (tris-buffered saline Tween; 20 mM Tris-HCl, 150 mM NaCl, 0.2 % (*v*/*v*) Tween-20). Membranes were incubated overnight with the anti-β-lactamase antibody (AB3738, Merck Millipore) diluted 1:5000 in 5 % (*w*/*v*) milk powder in TBST. The membranes were washed for 3 × 10 min in TBST. Membranes were then incubated with goat anti-rabbit IgG horseradish peroxidase conjugate (7074, New England Biolabs) diluted 1:10000 in TBST. Membranes were then washed 3 × 10 min in TBST before incubation with SuperSignal™ western pico chemiluminescent substrate (Thermo Fisher Scientific). The emitted signal was detected with Amersham hyperfilm (GE Healthcare).

### hIAPP, rIAPP, Aβ40 and Aβ42 purification or acquisition

Human and rat islet amyloid polypeptide were synthesized and purified as described previously[54] and kindly provided by Dr. Ling-Hsien Tu and Prof. Dan Raleigh (Stony Brook University, New York, USA). Synthetic Aβ42 was purchased from Invitrogen, catalogue number 03-112. Aβ40 was expressed in *E. coli* and purified as described previously[24].

### βla-linker and βla-hIAPP purification

BL21 (DE3) *E. coli* cells were transformed with the relevant plasmid and a single colony from a fresh transformation was used to inoculate 250 mL of LB medium containing 10 μg/mL tetracycline and incubated overnight at 37 °C with shaking at 200 rpm. 25 mL of overnight culture was then used to inoculate 10 × 1 L sterile LB containing 10 μg/mL tetracycline. The cultures were incubated at 37 °C with shaking (200 rpm) until an $OD_{600}$ of 0.6 was reached. Protein expression was then induced by the addition of filter-sterilized arabinose to a final concentration of 0.2 % (*w*/*v*). Cultures were incubated at 25 °C, 200 rpm, for 16 h. Cells were harvested in a Stratos continuous-flow rotor centrifuge at 15,000 rpm (HCT 22.300 Heraeus rotor).

The periplasmic fraction was extracted using the following procedure in a cold room using chilled reagents. The cell pellet was carefully resuspended in 20 mM Tris-HCl pH 8.0, 20 % (*w*/*v*) sucrose (4 mL of solution per gram of wet cell pellet). 1/100 volume of 100 × protease inhibitor cocktail (100 mM phenylmethylsulphonyl fluoride, 200 mM benzamidine, dissolved in EtOH) was added. 40 μL 0.5 M EDTA (Sigma) and 40 μL hen egg white lysozyme (Sigma) (10 mg/mL) were added per gram of wet cell pellet, and the sample left for 20 min on a shaker. 80 μL of 1 M $MgCl_2$ (per gram of wet cell pellet) was added to the

solution, and the cell suspension was centrifuged (20 min, 12,000 rpm, JA 25.50 Beckman-Coulter rotor, 4 °C) before the supernatant was collected.

The periplasmic fraction containing the β-lactamase construct was dialyzed overnight (3,500 MWCO membrane) against 5 L of 20 mM Tris-HCl, pH 7.5, 5 M urea at 4 °C with stirring. This process was repeated 3 times. The solution was filtered through a 0.2 μm syringe filter (Sartorius Stedim Biotech). The dialyzed periplasmic fraction obtained from 10 L of cells was loaded onto a 5 mL Hi Trap Q HP anion exchange column connected to an ÄKTA prime (GE Healthcare), equilibrated with three column volumes of 20 mM Tris-HCl, pH 7.5, 5 M urea (buffer A). The column was washed with three column volumes of buffer A before the protein was eluted with a linear gradient of 0–0.5 M NaCl, 20 mM Tris-HCl, pH 7.5, 5 M urea (Buffer B), maintaining the flow rate at 5 mL/min for all steps. 1.5 mL fractions were collected and the elution of protein monitored by absorbance at 280 nm. Fractions corresponding to the various peaks were analyzed by SDS PAGE. The fractions that contained the β-lactamase construct were pooled for further purification.

The desired fractions from anion exchange were concentrated to a final volume of 5 mL using an Amicon Ultra Centrifugal filter (10,000 MWCO). The sample (5 mL) was loaded onto a Superdex ™ 75 GL 10/300 gel filtration column (GE Healthcare), which had been equilibrated with 250 mL of 20 mM Tris-HCl, pH 7.5, 5 M urea. The protein was eluted from the column at a flow rate of 2 mL/min. 1.5 mL fractions were collected and the elution of protein monitored by absorbance at 280 nm. Fractions corresponding to the main peak were analyzed by SDS PAGE. The protein was refolded by dialysis into 200 mM ammonium acetate, pH 8 (typical yields from 1–2 mg/L pure protein were obtained). Protein identity was confirmed by mass spectrometry and protein was stored at −80 °C.

### Thioflavin T fluorometry

100 μL samples containing 100 μM thioflavin T and 50 μM protein in 200 mM ammonium acetate, pH 6.8 and a 1 % (*v*/*v*) final concentration of DMSO were prepared in a 96-well plate (CoStar) and sealed with clear sealing film (Breathe Easy, Sigma). Plates were incubated in a FLUOstar OPTIMA plate reader for 5 days at 25 °C without agitation. Fluorescence was excited using a 440 ± 5 nm filter, and emission intensity was measured using a 485 ± 5 nm filter.

### *In vitro* β-lactamase enzyme assay

The enzyme activity of βla-linker and βla-hIAPP was quantified spectrophotometrically using the colorimetric substrate nitrocefin. The assay was performed in a UV-1800 spectrophotometer (Shimadzu Ltd). In the absence of curcumin, 50 μL of 0.02 pmol/μL βla-linker or βla-hIAPP (in 50 mM sodium phosphate buffer, pH 7) was transferred to a clean quartz cuvette with a 1 cm path-length (Hellma Analytics). The reaction was started by the addition of 50 μL nitrocefin (100 μM stock solution in 50 mM sodium phosphate buffer, pH 7, 5 % (*v*/*v*) DMSO). Samples were base-line corrected using 50 μL of 50 mM sodium phosphate buffer, pH 7 with 50 μL nitrocefin stock. The change in absorbance at a wavelength of 486 nm was measured over 2 min at time intervals of 5 sec at room temperature. All determinations were carried out in triplicate. The initial rate of nitrocefin

hydrolysis was calculated (using the known molar extinction co-efficient of hydrolyzed nitrocefin ($\varepsilon$ = 20,500 $M^{-1}$ $cm^{-1}$)) and the specific activity was calculated as the amount of nitrocefin hydrolyzed per min per mg of enzyme (100 % activity).

In the presence of curcumin, the same assay conditions as above were used, however the enzyme stock solutions contained 0.2 pmol/μL curcumin (to give a final molar ratio of curcumin: enzyme of 10:1). The base-line was corrected using 50 μL of 0.2 pmol/μL curcumin in 50 mM sodium phosphate buffer, pH 7 and 50 μL nitrocefin stock.

### *In vitro* β-lactamase aggregation assay

βla-linker or βla-hIAPP (in 50 mM sodium phosphate buffer, pH 7) was added to wells of a 96-well plate (CoStar) to give a final enzyme concentration of 32 μM. 3.2 μL of 10 mM curcumin (in 100 % DMSO) was added to give a final small molecule concentration of 320 μM. For assays in the absence of curcumin, 3.2 μL of DMSO was added instead. Solutions were made up to 100 μL with 50 mM sodium phosphate buffer, pH 7 and the plates sealed with transparent, hydrophobic and gas permeable plastic films (Breathe Easy, Sigma). Plates were incubated for 5 days (quiescent, 25 °C). After 5 days, the enzyme activity of the whole sample was measured using a final enzyme concentration of 0.01 pmol/μL as described above. The samples were then centrifuged (1 h, 16,250 rpm, F-45-12-11 Eppendorf USA rotor) and the concentration of protein remaining in solution determined by the absorbance at 280 nm and the molar extinction coefficient of βla-linker (28,085 $M^{-1}$ $cm^{-1}$) or βla-hIAPP (29,700 $M^{-1}$ $cm^{-1}$) (samples were base-line corrected using 100 μL of 50 mM sodium phosphate buffer, pH 7, containing a final concentration of 320 μM curcumin, or an equivalent volume of DMSO). The enzyme assay was repeated and the amount of nitrocefin hydrolyzed per min mg of protein was calculated. The specific activity was calculated as a percentage of the initial specific activity (activity at t = 0 was 100 %).

### Transmission electron microscopy

Transmission electron microscope images were acquired on a *JEOL* JEM-1400 transmission electron microscope (JEOL Ltd.) after incubating 32 μM protein (βla-linker, βla-hIAPP, rIAPP, hIAPP, Aβ40, or Aβ42) solutions in the presence or absence of 320 μM small molecule for 5 days at 25 °C, quiescent. Carbon grids were prepared by irradiating under UV light for 30 min and samples were stained with 4 % (*w*/*v*) uranyl acetate (Sigma) solution.

### Characterization of βla-hIAPP aggregates as amyloid

Fluorescence emission spectra of 50 μM βla-linker, βla-hIAPP or hIAPP (in 200 mM ammonium acetate, pH 6.8, 1 % (*v*/*v*) DMSO) were recorded after 5 days incubation by the addition of 10 μM of the amyloid-specific dyes NIAD-4 (ChemShuttle) or ThT (Sigma). Spectra were aquired using a Photon Technology International fluorimeter (Ford). NIAD-4 emission spectra were recorded between 500 nm to 800 nm using an excitation wavelength of 490 nm with excitation and emission slit widths of 3 nm and 4 nm, respectively. ThT emission spectra were recorded between 460 nm and 800 nm using an excitation wavelength of 440 nm with excitation and emission slit widths of 2 nm and 3 nm, respectively.

Dot-blots were performed using 10 μL of 50 μM of each protein incubated for 5 days, as described above. Proteins were transferred to Amersham nitrocellulose using a SCIE-PLAS dot-blotting manifold. Blocking was performed for 3 h at room temperature using 5 % (*w*/*v*) BSA in TBST. Membranes were incubated overnight with the anti-amyloid antibody WO1 (a gift from R. Wetzel, University of Pittsburgh, USA) diluted 1:5000 in 5 % (*w*/*v*) BSA in TBST or 5 % (*w*/*v*) BSA in TBST with no primary antibody as a control. The membranes were washed for 3 × 10 min in TBST. Membranes were then incubated with rat anti-mouse IgM horseradish peroxidase conjugate (BD Biosciences) diluted 1:7500 in TBST. Membranes were then washed 3 × 10 min in TBST before incubation with SuperSignal™ western pico chemiluminescent substrate (Thermo Fisher Scientific). The emitted signal was detected with Amersham hyperfilm (GE Healthcare).

## Mass spectrometry sample preparation

Lyophilized hIAPP and rIAPP samples were dissolved in DMSO to a concentration of 3.2 mM. After 24 h incubation at 25 °C, stock solutions were diluted in 200 mM ammonium acetate, pH 6.8, to give a final peptide concentration of 32 μM for mass spectrometry analysis. The final concentration of DMSO was 1 % (*v*/*v*). Lyophilized Aβ40 and Aβ42 were dissolved at 32 μM in 200 mM ammonium acetate, pH 6.8, 1 % DMSO (*v*/*v*). The Aβ40 and Aβ42 peptide samples were centrifuged (13,000 rpm, F-45-12-11 Eppendorf USA rotor, 4 °C, 10 min) before analysis. All samples were incubated at 25 °C in 96-well plates without agitation.

300 μM βla-hIAPP or βla-linker stock solution (in 200 mM ammonium acetate, pH 8) was buffer exchanged using 0.5 mL Zeba buffer exchange columns (Thermo Fischer Scientific) equilibrated with 200 mM ammonium acetate, pH 6.8. The sample was diluted to a final concentration of 50 μM for mass spectrometry analysis.

## ESI-(IMS)-MS analysis

A Synapt HDMS quadrupole-time-of-flight mass spectrometer (Waters Corpn.), equipped with a Triversa NanoMate (Advion Biosciences) automated nano-ESI interface, was used for the analyses. The instrument has a traveling-wave IMS device situated between the quadrupole and the time-of-flight analyzers, and has been described in detail elsewhere[55]. rIAPP, hIAPP, Aβ40 or Aβ42 samples were analyzed using positive ionization nanoESI (nESI) with a capillary voltage of 1.7 kV and a nitrogen nebulizing gas pressure of 0.8 psi. The following instrumental parameters were used: cone voltage 30 V; source temperature 60 °C; backing pressure 1.6 mBar; ramped traveling wave height 7–20 V; traveling wave speed 300 m/s; IMS nitrogen gas flow 20 mL/min; IMS cell pressure 0.55 mBar. Data were processed by use of MassLynx v4.1 and Driftscope software supplied with the mass spectrometer. The *m*/*z* scale was calibrated with aq. CsI cluster ions.

For ESI-IMS-MS time course experiments, 50 μM peptide samples were incubated in 200 mM ammonium acetate buffer, pH 6.8, 1 % (*v*/*v*) DMSO for 2 min or 24 h. 10 μL volumes were removed from each solution and infused into the mass spectrometer for analysis.

### Mass spectrometry analysis of ligand binding to monomeric protein

hIAPP (32 μM) in 200 mM ammonium acetate (pH 6.8) containing 320 μM of small molecule was analyzed by ESI-MS using a sampling cone voltage of 30 V to preserve protein-ligand interactions, and a backing pressure of 1.6 mBar. Data were acquired over the range *m*/*z* 100–6,000, and processed by use of MassLynx v4.1 and Driftscope software supplied with the mass spectrometer. The *m*/*z* scale was calibrated with aq. CsI cluster ions.

10 mM stock of small molecule (dissolved in DMSO, EtOH or $H_2O$) was added to solutions of βla-linker or βla-hIAPP (in 200 mM ammonium acetate, pH 6.8) to give a final small molecule: βla-linker/βla-hIAPP concentration of 500:50 μM. The following instrumental parameters were used: cone voltage 30 V; source temperature 60 °C; backing pressure 4.0 mBar; ramped traveling wave height 7–20 V; traveling wave speed 300 m/s; IMS nitrogen gas flow 20 mL/min; IMS cell pressure 0.55 mBar.

### Virtual screening for small molecules

The structure of a recently identified inhibitor of hIAPP aggregation, JCS-1 (compound **36**; 6-[4-(2-fluorophenyl)-1-piperazinyl]-carbonyl-3-methyl-5*H*-[1,3]-thiazolo[3,2-a]pyrimidin-5-one)[24], was minimized to the lowest energy conformer using LigPrep[56]. The minimized conformer was used as the query scaffold for virtual screening of an in-house library of 50,000 structurally diverse, novel small molecules using Rapid Overlay of Chemical Structures (ROCS)[57]. ROCS is a 3D method that matches the shape of a molecule to the shape of the query molecule. It also incorporates pharmacophoric features in assessing overlays such that the *ROCS Combiscore* measures the similarity of the matched shapes as well as the matched pharmacophoric features. Virtual hits were pooled and ranked according to the *ROCS Combiscore* parameter and 28 were selected for screening based on a qualitative assessment of structural diversity.

## Supplementary Material

Refer to Web version on PubMed Central for supplementary material.

## Acknowledgements

J.C.S. is funded by Innovate UK (131841) and the Biotechnology and Biological Sciences Research Council (BBSRC) (BB/M01259X/1) and was previously funded by a BBSRC CASE studentship (Grant Number BB/H014713/1) sponsored by Avacta Analytical plc, Wetherby, UK. L.M.Y. is funded by a BBSRC CASE studentship (Grant Number BB/I015361/1) sponsored by Micromass UK Ltd/Waters Corpn., Manchester, UK. R.A.M. is funded by a BBSRC studentship (Grant Number BB/F01614X/1). The Synapt HDMS mass spectrometer was purchased with funds from the BBSRC (BB/E012558/1). M.P.J., D.J.B. and S.E.R. also acknowledge funding from the European Research Council under the European Union's Seventh Framework Programme (*FP7/2007-2013*) / ERC grant agreement number 322408. R.J.F. and C.H.R. acknowledge the Biomedical Health Research Centre (University of Leeds) for funding. We thank Professor Jim Bardwell (University of Michigan) for his longstanding collaboration and advice at the beginning of the study. We thank Dr Simon Webster (Avacta Analytical plc) for his advice and helpful discussions. We are very grateful to Professor Dan Raleigh and Dr Ling-Hsien Tu (Stoney Brook University) for kindly providing the synthetic hIAPP and rIAPP peptides. We thank Professor Ronald Wetzel (University of Pittsburgh) for providing the WO1 antibody. We also acknowledge our collaborators and all members of our groups for helpful discussions.

D.A.S is Chief Executive of Avacta Analytical plc.

## References for main text


1. Sipe JD, et al. Nomenclature 2014: Amyloid fibril proteins and clinical classification of the amyloidosis. Amyloid. 2014; 21:221–224. (doi:10.3109/13506129.2014.964858). [PubMed: 25263598]
2. Knowles TPJ, Vendruscolo M, Dobson CM. The amyloid state and its association with protein misfolding diseases. Nat. Rev. Mol. Cell. Biol. 2014; 15:384–396. (10.1038/nrm3810). [PubMed: 24854788]
3. Tipping KW, Oosten-Hawle P.v. Hewitt EW, Radford SE. Amyloid fibres: inert end-stage aggregates or key players in disease? Trends Biochem. Sci. 2015 (http://dx.doi.org/10.1016/j.tibs.2015.10.002).
4. Pieri L, Madiona K, Bousset L, Melki R. Fibrillar α-synuclein and huntingtin exon 1 assemblies are toxic to the cells. Biophys. J. 2012; 102:2894–2905. (10.1016/j.bpj.2012.04.050). [PubMed: 22735540]
5. Bulawa CE, et al. Tafamidis, a potent and selective transthyretin kinetic stabilizer that inhibits the amyloid cascade. Proc. Natl. Acad. Sci. U. S. A. 2012; 109:9629–9634. (10.1073/pnas.1121005109). [PubMed: 22645360]
6. Meng F, Marek P, Potter KJ, Verchere CB, Raleigh DP. Rifampicin does not prevent amyloid fibril formation by human islet amyloid polypeptide but does inhibit fibril thioflavin-T interactions: implications for mechanistic studies of β-cell death. Biochem. 2008; 47:6016–6024. (10.1021/bi702518m). [PubMed: 18457428]
7. Butterfield S, Hejjaoui M, Fauvet B, Awad L, Lashuel HA. Chemical strategies for controlling protein folding and elucidating the molecular mechanisms of amyloid formation and toxicity. J. Mol. Biol. 2012; 421:204–236. [PubMed: 22342932]
8. Foit L, et al. Optimizing protein stability *in vivo*. Mol. Cell. 2009; 36:861–871. (10.1016/j.molcel.2009.11.022). [PubMed: 20005848]
9. Kim W, et al. A high-throughput screen for compounds that inhibit aggregation of the Alzheimer's peptide. ACS Chem. Biol. 2006; 1:461–469. (10.1021/cb600135w). [PubMed: 17168524]
10. Lee LL, Ha H, Chang YT, DeLisa MP. Discovery of amyloid-beta aggregation inhibitors using an engineered assay for intracellular protein folding and solubility. Protein Sci. 2009; 18:277–286. (10.1002/pro.33). [PubMed: 19177561]
11. Espargaro A, Sabate R, Ventura S. Thioflavin-S staining coupled to flow cytometry. A screening tool to detect *in vivo* protein aggregation. Mol. Biosyst. 2012; 8:2839–2844. [PubMed: 22868714]
12. Romero D, Sanabria-Valentín E, Vlamakis H, Kolter R. Biofilm inhibitors that target amyloid proteins. Chem. Biol. 2013; 20:102–110. [PubMed: 23352144]
13. McKoy AF, Chen J, Schupbach T, Hecht MH. A novel inhibitor of amyloid β (Aβ) peptide aggregation: from high throughput screening to efficacy in an animal model of Alzheimer disease. J. Biol. Chem. 2012; 287:38992–39000. (10.1074/jbc.M112.348037). [PubMed: 22992731]
14. Morell M, de Groot NS, Vendrell J, Aviles FX, Ventura S. Linking amyloid protein aggregation and yeast survival. Mol. Biosyst. 2011; 7:1121–1128. [PubMed: 21240401]
15. Nikaido H. Molecular basis of bacterial outer membrane permeability revisited. Microbiol. Mol. Biol. Rev. 2003; 67:593–656. (10.1128/mmbr.67.4.593-656.2003). [PubMed: 14665678]
16. Hailu TT, Foit L, Bardwell JCA. *In vivo* detection and quantification of chemicals that enhance protein stability. Anal. Biochem. 2013; 434:181–186. [PubMed: 23219982]
17. Quan S, et al. Genetic selection designed to stabilize proteins uncovers a chaperone called Spy. Nat. Struct. Mol. Biol. 2011; 18:262–269. [PubMed: 21317898]
18. Chen Y-R, Glabe CG. Distinct early folding and aggregation properties of Alzheimer amyloid-β peptides Aβ40 and Aβ42: stable trimer or tetramer formation by Aβ42. J. Biol. Chem. 2006; 281:24414–24422. (10.1074/jbc.M602363200). [PubMed: 16809342]
19. Bitan G, Lomakin A, Teplow DB. Amyloid β-protein oligomerization: prenucleation interactions revelaed by photo-induced cross-linking of unmodified proteins. J. Biol. Chem. 2001; 276:35176–35184. (10.1074/jbc.M102223200). [PubMed: 11441003]
20. Young LM, Cao P, Raleigh DP, Ashcroft AE, Radford SE. Ion mobility spectrometry–mass spectrometry defines the oligomeric intermediates in amylin amyloid formation and the mode of

action of inhibitors. J. Am. Chem. Soc. 2013; 136:660–670. (10.1021/ja406831n). [PubMed: 24372466]

21. Koo BW, Miranker AD. Contribution of the intrinsic disulfide to the assembly mechanism of islet amyloid. Protein Sci. 2005; 14:231–239. (10.1110/ps.041051205). [PubMed: 15576552]
22. Qiao Q, Bowman GR, Huang X. Dynamics of an intrinsically disordered protein reveal metastable conformations that potentially seed aggregation. J. Am. Chem. Soc. 2013; 135:16092–16101. (10.1021/ja403147m). [PubMed: 24021023]
23. Sgourakis NG, Yan Y, McCallum SA, Wang C, Garcia AE. The Alzheimer's peptides Aβ40 and 42 adopt distinct conformations in water: a combined MD / NMR study. J. Mol. Biol. 2007; 368:1448–1457. [PubMed: 17397862]
24. Young LM, et al. Screening and classifying small molecule inhibitors of amyloid formation using ion mobility spectrometry-mass spectrometry. Nat. Chem. 2015; 7:73–81. [PubMed: 25515893]
25. Nesterov EE, et al. *In vivo* optical imaging of amyloid aggregates in brain: design of fluorescent markers. Angew. Chem. Int. Ed. 2005; 44:5452–5456. (10.1002/anie.200500845).
26. O'Nuallain B, Wetzel R. Conformational Abs recognizing a generic amyloid fibril epitope. Proc. Natl. Acad. Sci. U. S. A. 2002; 99:1485–1490. (10.1073/pnas.022662599). [PubMed: 11818542]
27. Eichner T, Kalverda AP, Thompson GS, Homans SW, Radford SE. Conformational conversion during amyloid formation at atomic resolution. Mol. Cell. 2011; 41:161–172. [PubMed: 21255727]
28. Valleix S, et al. Hereditary systemic amyloidosis due to Asp76Asn variant $\beta_2$-microglobulin. N. Engl. J. Med. 2012; 366:2276–2283. (doi:10.1056/NEJMoa1201356). [PubMed: 22693999]
29. Mangione PP, et al. Structure, folding dynamics, and amyloidogenesis of D76N β2-microglobulin: roles of shear flow, hydrophobic surfaces, and α-crystallin. J. Biol. Chem. 2013; 288:30917–30930. (10.1074/jbc.M113.498857). [PubMed: 24014031]
30. Jespers L, Schon O, Famm K, Winter G. Aggregation-resistant domain antibodies selected on phage by heat denaturation. Nat. Biotechnol. 2004; 22:1161–1165. [PubMed: 15300256]
31. Jespers L, Schon O, James LC, Veprintsev D, Winter G. Crystal structure of HEL4, a soluble, refoldable human $V_H$ single domain with a germ-line scaffold. J. Mol. Biol. 2004; 337:893–903. [PubMed: 15033359]
32. Daval M, et al. The effect of curcumin on human islet amyloid polypeptide misfolding and toxicity. Amyloid. 2010; 17:118–128. (doi:10.3109/13506129.2010.530008). [PubMed: 21067307]
33. Sparks S, Liu G, Robbins KJ, Lazo ND. Curcumin modulates the self-assembly of the islet amyloid polypeptide by disassembling α-helix. Biochem. Biophys. Res. Commun. 2012; 422:551–555. [PubMed: 22579683]
34. Meng F, et al. The sulfated triphenyl methane derivative acid fuchsin is a potent inhibitor of amyloid formation by human islet amyloid polypeptide and protects against the toxic effects of amyloid formation. J. Mol. Biol. 2010; 400:555–566. [PubMed: 20452363]
35. Meng F, Raleigh DP. Inhibition of glycosaminoglycan-mediated amyloid formation by islet amyloid polypeptide and proIAPP processing intermediates. J. Mol. Biol. 2010; 406:491–502. [PubMed: 21195086]
36. Palhano FL, Lee J, Grimster NP, Kelly JW. Toward the molecular mechanism(s) by which EGCG treatment remodels mature amyloid fibrils. J. Am. Chem. Soc. 2013; 135:7503–7510. [PubMed: 23611538]
37. Cheng B, et al. Coffee components inhibit amyloid formation of human islet amyloid polypeptide *in vitro*: possible link between coffee consumption and diabetes mellitus. J. Agric. Food Chem. 2011; 59:13147–13155. (10.1021/jf201702h). [PubMed: 22059381]
38. Cheng B, et al. Silibinin inhibits the toxic aggregation of human islet amyloid polypeptide. Biochem. Biophys. Res. Commun. 2012; 419:495–499. (10.1016/j.bbrc.2012.02.042). [PubMed: 22366091]
39. Tu L-H, et al. Mutational analysis of the ability of resveratrol to inhibit amyloid formation by islet amyloid polypeptide: critical evaluation of the importance of aromatic–inhibitor and histidine–inhibitor interactions. Biochem. 2014; 54:666–676. (10.1021/bi501016r). [PubMed: 25531836]

40. Aitken JF, Loomes KM, Konarkowska B, Cooper GJS. Suppression by polycyclic compounds of the conversion of human amylin into insoluble amyloid. Biochem. J. 2003; 374:779–784. (10.1042/bj20030422). [PubMed: 12812521]
41. Aarabi MH, Mirhashemi SM. The role of two natural flavonoids on human amylin aggregation. Afr. J. Ph. Pharmacol. 2012; 6:2374–2379. (citeulike-article-id:11399209 doi: 10.5897/AJPP12.616).
42. Zelusa C, et al. Myricetin inhibits islet amyloid polypeptide (IAPP) aggregation and rescues living mammalian cells from IAPP toxicity. Open Biochem. J. 2012; 6:66–70. [PubMed: 22792130]
43. Porat Y, Mazor Y, Efrat S, Gazit E. Inhibition of islet amyloid polypeptide fibril formation: a potential role for heteroaromatic interactions. Biochem. 2004; 43:14454–14462. (10.1021/bi048582a). [PubMed: 15533050]
44. Wu C, Lei H, Wang Z, Zhang W, Duan Y. Phenol red interacts with the protofibril-like oligomers of an amyloidogenic hexapeptide NFGAIL through both hydrophobic and aromatic contacts. Biophys. J. 2006; 91:3664–3672. [PubMed: 16935948]
45. Noor H, Cao P, Raleigh DP. Morin hydrate inhibits amyloid formation by islet amyloid polypeptide and disaggregates amyloid fibers. Protein Sci. 2012; 21:373–382. (10.1002/pro.2023). [PubMed: 22238175]
46. Li J, Zhu M, Manning-Bog AB, Di Monte DA, Fink AL. Dopamine and L-dopa disaggregate amyloid fibrils: implications for Parkinson's and Alzheimer's disease. FASEB J. 2004; 18:962–964. (10.1096/fj.03-0770fje). [PubMed: 15059976]
47. Lee H-J, et al. Dopamine promotes formation and secretion of non-fibrillar alpha-synuclein oligomers. Exp. Mol. Med. 2011; 43:216–222. [PubMed: 21415592]
48. Baell J, W.M. Chemistry: Chemical con artists foil drug discovery. Nature. 2014; 513:481–483. [PubMed: 25254460]
49. Baell JB, Holloway GA. New substructure filters for removal of Pan Assay Interference Compounds (PAINS) from screening libraries and for their exclusion in bioassays. J. Med. Chem. 2010; 53:2719–2740. (10.1021/jm901137j). [PubMed: 20131845]

## Methods-only references

8. Foit L, et al. Optimizing protein stability *in vivo*. Mol. Cell. 2009; 36:861–871. (10.1016/j.molcel.2009.11.022). [PubMed: 20005848]
24. Young LM, et al. Screening and classifying small molecule inhibitors of amyloid formation using ion mobility spectrometry-mass spectrometry. Nat. Chem. 2015; 7:73–81. [PubMed: 25515893]
50. Jelsch C, Mourey L, Masson J-M, Samama J-P. Crystal structure of *Escherichia coli* TEM1 β-lactamase at 1.8 Å resolution. Proteins: Struct., Funct., Bioinf. 1993; 16:364–383. (10.1002/prot.340160406).
51. Williamson JA, Miranker AD. Direct detection of transient α-helical states in islet amyloid polypeptide. Protein Sci. 2007; 16:110–117. (10.1110/ps.062486907). [PubMed: 17123962]
52. Walsh DM, et al. A facile method for expression and purification of the Alzheimer's disease-associated amyloid β-peptide. FEBS J. 2009; 276:1266–1281. (10.1111/j.1742-4658.2008.06862.x). [PubMed: 19175671]
53. Kad NM, Thomson NH, Smith DP, Smith DA, Radford SE. β2-microglobulin and its deamidated variant, N17D form amyloid fibrils with a range of morphologies in vitro. J. Mol. Biol. 2001; 313:559–571. [PubMed: 11676539]
54. Marek P, Woys AM, Sutton K, Zanni MT, Raleigh DP. Efficient microwave-assisted synthesis of human islet amyloid polypeptide designed to facilitate the specific incorporation of labeled amino acids. Org. Lett. 2010; 12:4848–4851. (10.1021/ol101981b). [PubMed: 20931985]
55. Giles K, et al. Applications of a travelling wave-based radio-frequency-only stacked ring ion guide. Rapid Commun. Mass Spectrom. 2004; 18:2401–2414. (10.1002/rcm.1641). [PubMed: 15386629]
56. Schrödinger Release. Edn. 9.3. Schrödinger, LLC; NY, USA: 2014-2.
57. OpenEye, Scientific Software; Santa Fe, NM, USA: http://www.eyesopen.com/

Europe PMC Funders Author Manuscripts

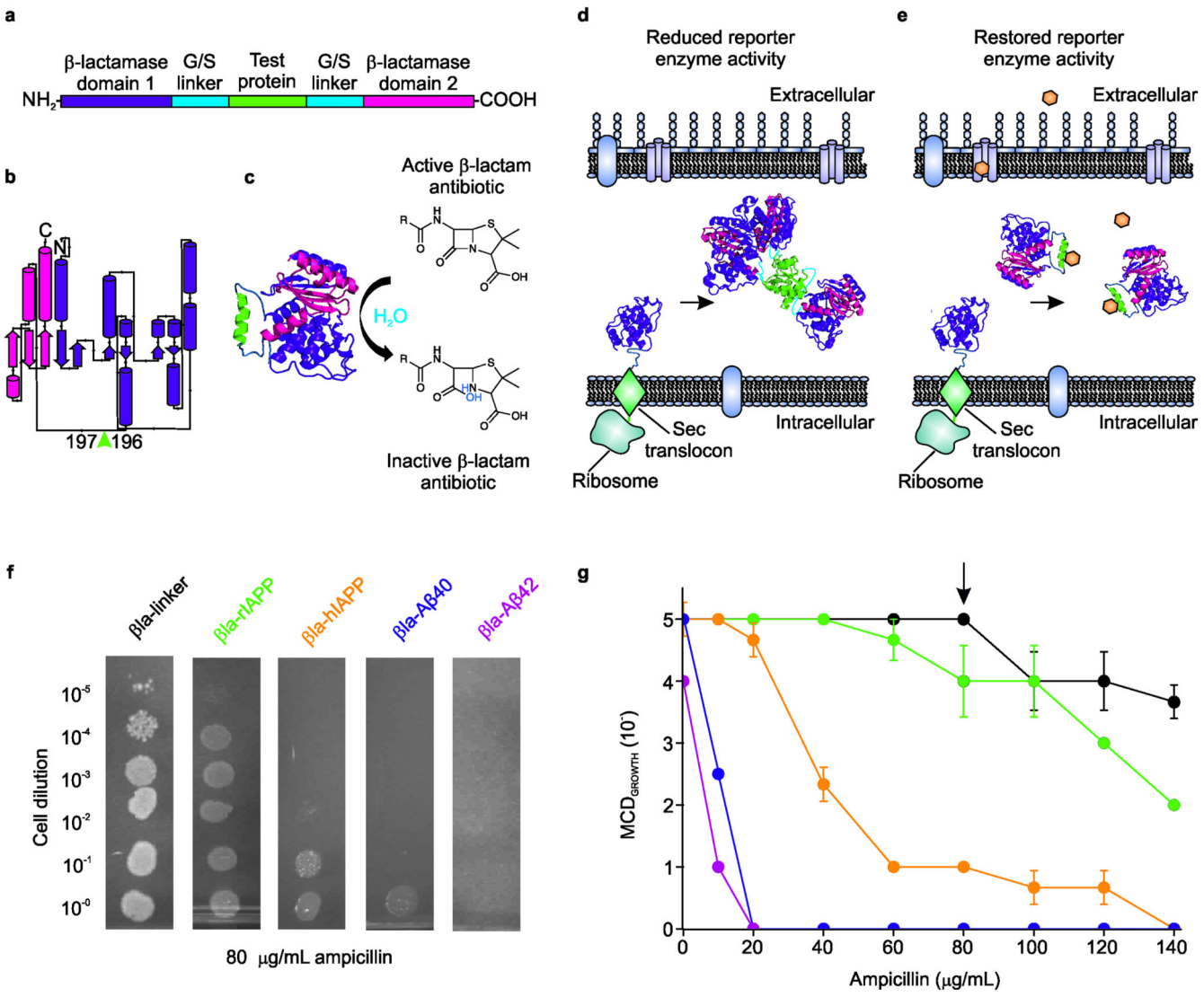


**Figure 1.**

Split β-lactamase assay for protein aggregation identifies aggregation-prone sequences. (**a**–**e**) Schematic of the split β-lactamase assay for protein aggregation. (**a**) The test protein (green) is inserted into a glycine/serine-rich linker (blue) within the loop region separating the two domains of TEM-1 β-lactamase (purple and pink). (**b**) Topology of TEM-1 β-lactamase highlighting the insertion point (green arrow) of the glycine/serine-rich linker between residues 196 and 197 (figure created using online database PDBsum and PDB entry 1BTL[50]). (**c**) Association of the two β-lactamase domains results in the formation of the enzyme active site. (**d**) If the test protein aggregates, the activity of β-lactamase is reduced and the bacteria become more sensitive to β-lactam antibiotics. (**e**) Small molecule inhibitors (yellow) of protein aggregation diffuse into the periplasm via porins and prevent aggregation of the β-lactamase tripartite fusion protein, restoring bacterial resistance to β-lactam antibiotics. (**f**) Spot titer of bacteria expressing βla-linker (black), βla-rIAPP (green), βla-hIAPP (orange), βla-Aβ40 (purple) or βla-Aβ42 (pink) on agar containing 80 μg/mL

ampicillin. (**g**) Antibiotic survival curve of the maximal cell dilution allowing growth ($MCD_{GROWTH}$) after 18 h over a range of ampicillin concentrations for each of the tripartite fusion constructs, colored as in (**f**). Data represent mean values ± s.e.m (n = 4 replicate experiments). The arrow depicts the ampicillin concentration used in (**f**).



Europe PMC Funders Author Manuscripts

Europe PMC Funders Author Manuscripts

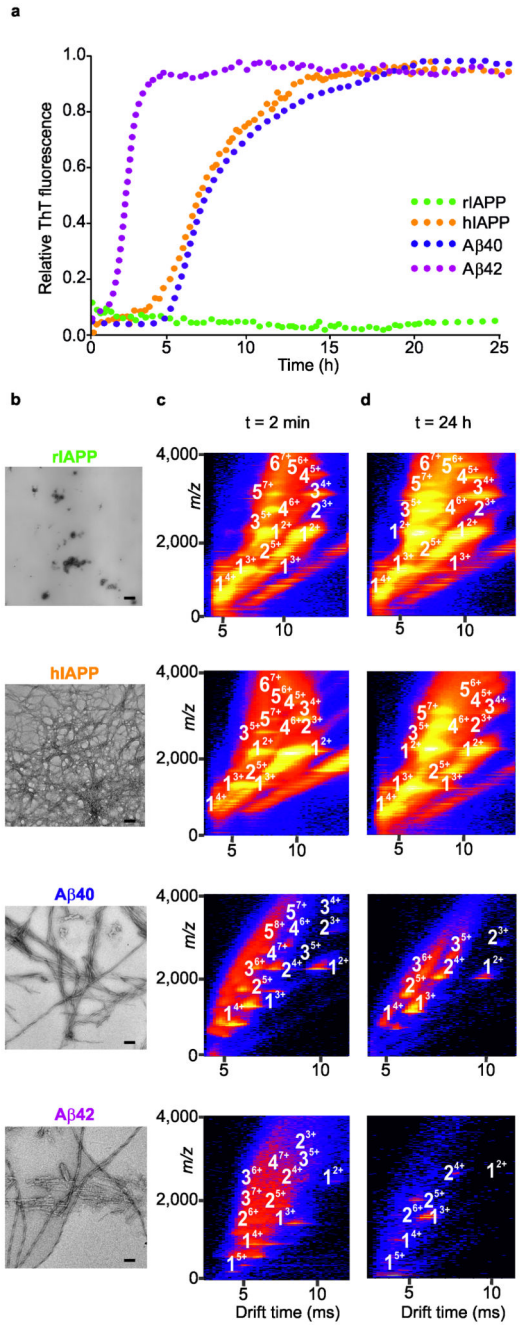


**Figure 2.**

Antibiotic resistance of the tripartite fusion constructs correlates with peptide aggregation propensity *in vitro*. ThT fluorescence intensity (**a**), negative stain TEM images (**b**) and ESI-IMS-MS Driftscopes taken at 2 min (**c**) or 24 h (**d**) of aggregates formed by rIAPP, hIAPP, Aβ40 and Aβ42. ThT fluorescence measured over 24 h. TEM images acquired after 5 days. Scale bar = 100 nm. Driftscope plots (drift-time vs. *m*/*z* vs. intensity) show extent of oligomerization after 2 min or 24 h. The numbers on the Driftscope plots indicate the oligomer order and the adjacent superscript numbers show the charge state of those ions.

Europe PMC Funders Author Manuscripts

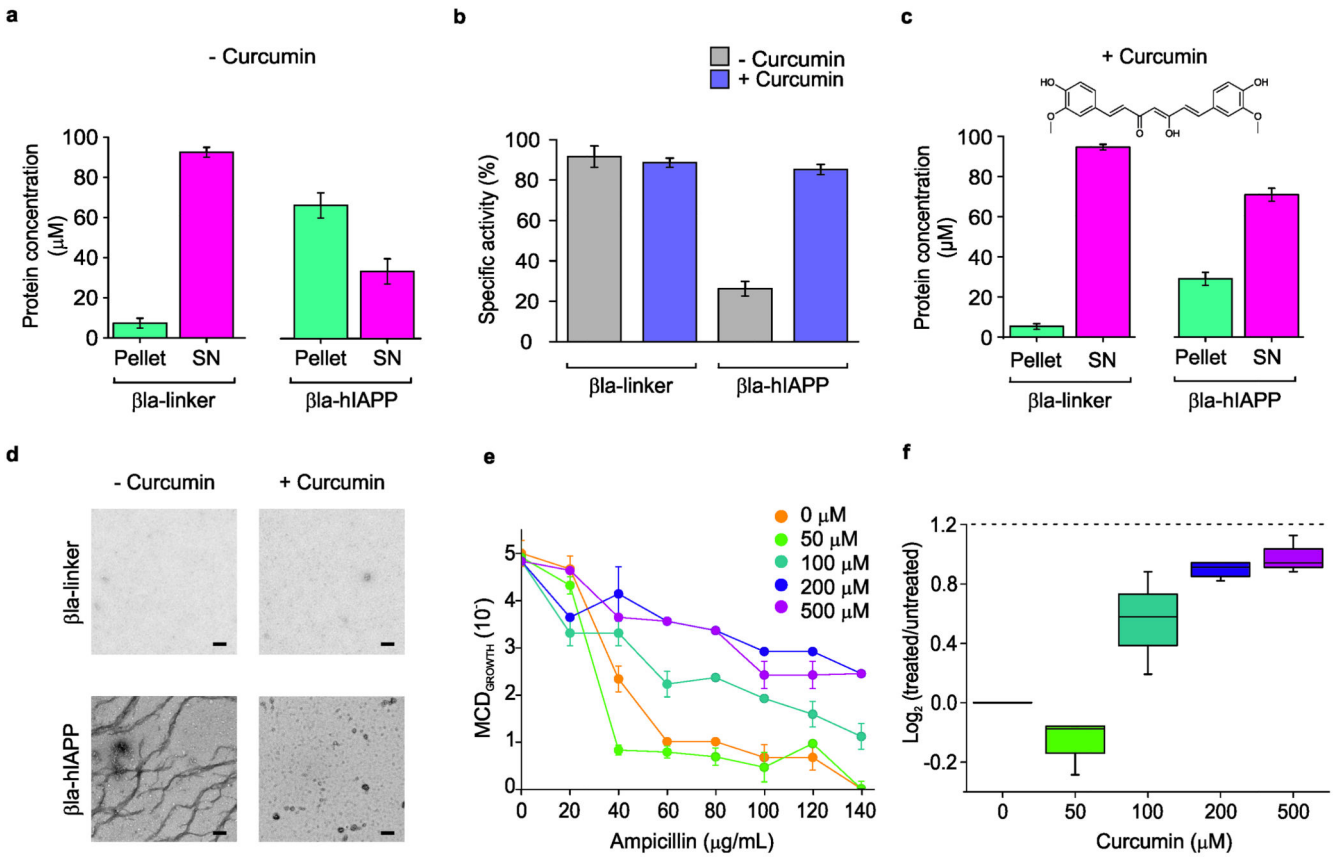


**Figure 3.**

βla-hIAPP aggregation *in vitro* and the effects of curcumin *in vitro* and *in vivo*. (**a**) Concentration of βla-linker or βla-hIAPP in the pellet (turquoise) or supernatant (SN, pink) after 5 days. (**b**) Specific enzyme activity (μmol nitrocefin hydrolyzed per min per mg of enzyme) of the whole sample at the end of the 5 day incubation ± a 10-fold molar excess of curcumin (32:320 μM). Specific activity at 0 days is defined as 100 %. Data are presented as mean values ± s.e.m, n = 4 independent experiments. (**c**) Concentration of βla-linker or βla-hIAPP in the pellet or SN after 5 days incubation in the presence of a 10-fold molar excess of curcumin (structure inset). (**d**) TEM analysis of aggregates formed by βla-linker or βla-hIAPP ± curcumin after the 5 days incubation (scale bar = 100 nm). (**e**) Antibiotic survival curve showing the maximal cell dilution allowing growth ($MCD_{GROWTH}$) of bacteria expressing the βla-hIAPP construct in the presence of increasing concentrations of curcumin (0–500 μM) (n = 4 replicate experiments). Data were plotted after toxicity of curcumin was accounted (see online Methods and Supplementary Fig. 6). (**f**) Data plotted as $\log_2$(treated/untreated) growth, calculated from the areas under the antibiotic survival curves in (**e**); see online Methods equation (1). Center line = median; box limits = 25$^{th}$ and 75$^{th}$ percentiles (whiskers extending to ± 1.5 × IQR), n = 4. 100 % rescue is equivalent to $\log_2$(treated/untreated) = 1.2 (indicated by dotted line).

Europe PMC Funders Author Manuscripts

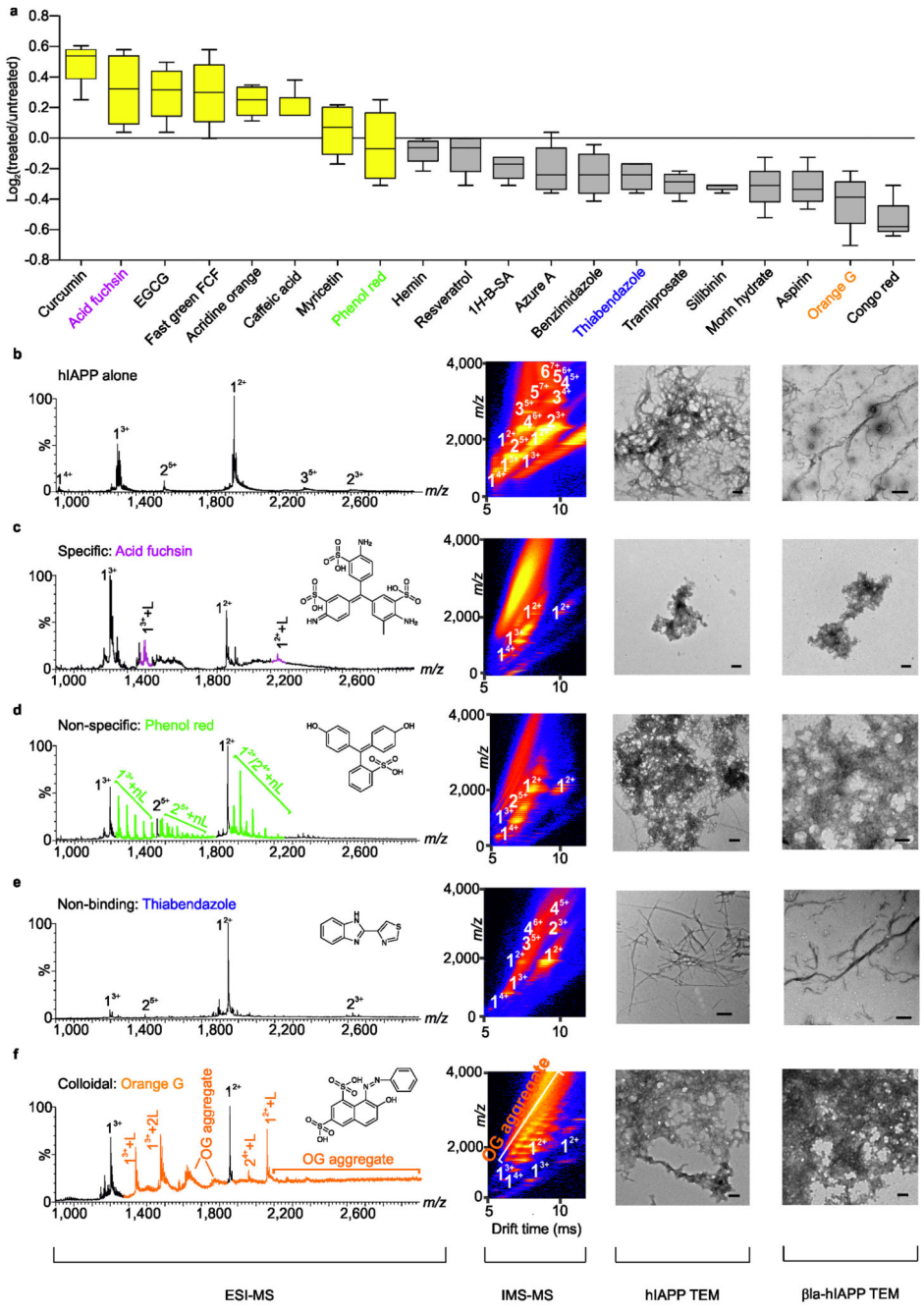


**Figure 4.**

*In vivo* screen identifies hIAPP aggregation inhibitors. (**a**) Effect of 100 μM small molecule on bacterial growth, quantified by $\log_2$(treated /untreated) (n = 4). Data were calculated from the areas under the antibiotic survival curves, after the toxicity of the small molecule on bacterial growth was accounted for by analysis of the effect of each small molecule on the growth of cells expressing βla-linker (online Methods and Supplementary Fig. 6). Center line = median; box limits = 25$^{th}$ and 75$^{th}$ percentiles (whiskers extending to ± 1.5 × IQR). Black line indicates separation of hits (> 0, yellow) from non-hits (≤ 0, grey). In this format,

100 % rescue is equivalent to $\log_2$(treated/untreated) = 1.2. (**b–f**) ESI-MS mass spectra (left), IMS-MS Driftscope plots (middle) and negative statin TEM images (middle-right) of hIAPP peptide in the absence (**b**) or presence of acid fuchsin (**c**), phenol red (**d**), thiabendazole (**e**) or Orange G (**f**). Positive ion ESI mass spectra label $X^{y+}$ denotes the oligomer order (X) and charge state of the species (y+). $X^{y+}$ + nL denotes the number (n) of ligands (L) bound to the particular $X^{y+}$ charge state. (**b–e**, far-right) Negative stain TEM images of aggregates formed by βla-hIAPP ± the same small molecules. TEM images taken after 5 days incubation. Scale bar = 100 nm.



Europe PMC Funders Author Manuscripts

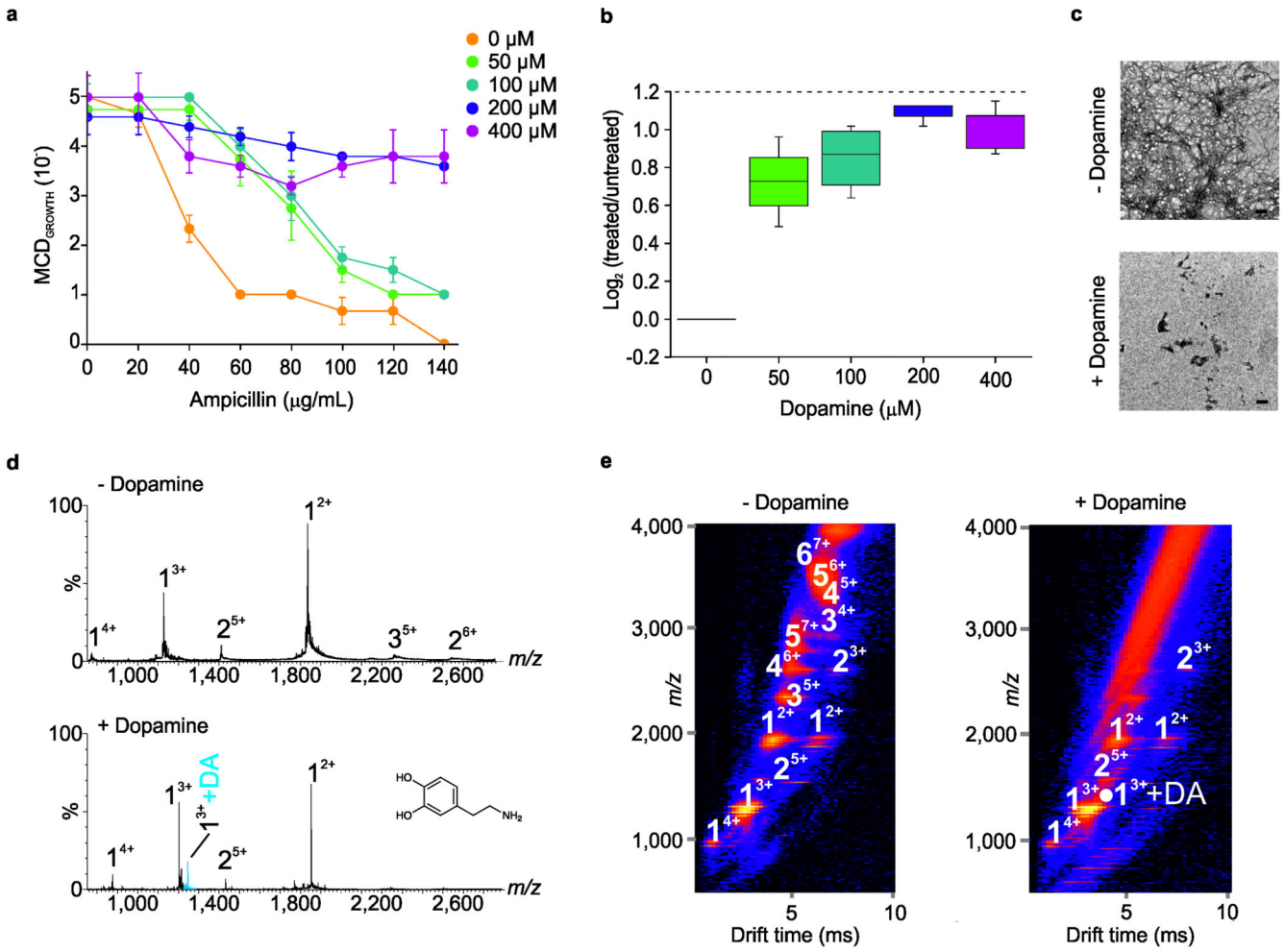


**Figure 5.**

Identification of dopamine as an inhibitor of hIAPP aggregation. (**a**) Antibiotic survival curve showing the effect of dopamine (0–400 μM) on growth of bacteria expressing the βla-hIAPP construct (n = 4 replicate experiments). (**b**) Data plotted as $\log_2$(treated/untreated), calculated from the areas under the antibiotic survival curves in (**b**); see online Methods, equation (1). Center line = median; box limits = 25$^{th}$ and 75$^{th}$ percentiles (whiskers extending to ± 1.5 × IQR). In this format, 100 % rescue is equivalent to $\log_2$(treated/untreated) = 1.2 (indicated by dotted line). (**c**) Negative stain TEM analysis of aggregates formed by hIAPP ± dopamine after 5 days incubation. Scale bar = 100 nm. (**d**) ESI mass spectra showing hIAPP alone (**i**) or in the presence of a 10-fold excess of dopamine (structure inset). (**e**) ESI–IMS–MS Driftscope plots of hIAPP ± dopamine. The numbers on the Driftscope plots indicate the oligomer order and the adjacent superscript numbers show the charge state of those ions. White circle indicates dopamine bound to hIAPP.




Europe PMC Funders Author Manuscripts